ADVANCES IN ATMOSPHERIC SCIENCES, VOL. 32, NOVEMBER 2015, 1460–1472

An Ocean Data Assimilation System in the Indian Ocean and West Pacific Ocean

YAN Changxiang*, ZHU Jiang, and XIE Jiping

International Center for Climate and Environment Sciences, Institute of Atmospheric Physics, Chinese Academy of Sciences, Beijing 100029

(Received 15 November 2014; revised 16 April 2015; accepted 30 April 2015)

ABSTRACT

The development and application of a regional ocean data assimilation system are among the aims of the Global Ocean Data Assimilation Experiment. The ocean data assimilation system in the regions including the Indian and West Pacific oceans is an endeavor motivated by this goal. In this study, we describe the system in detail. Moreover, the reanalysis in the joint area of Asia, the Indian Ocean, and the western Pacific Ocean (hereafter AIPOcean) constructed using multi-year model integration with data assimilation is used to test the performance of this system. The ocean model is an eddy-resolving, hybrid coordinate ocean model. Various types of observations including *in-situ* temperature and salinity profiles (mechanical bathythermograph, expendable bathythermograph, Array for Real-time Geostrophic Oceanography, Tropical Atmosphere Ocean Array, conductivity–temperature–depth, station data), remotely-sensed sea surface temperature, and altimetry sea level anomalies, are assimilated into the reanalysis via the ensemble optimal interpolation method. An ensemble of model states sampled from a long-term integration is allowed to change with season, rather than remaining stationary. The estimated background error covariance matrix may reasonably reflect the seasonality and anisotropy. We evaluate the performance of AIPOcean during the period 1993–2006 by comparisons with independent observations, and some reanalysis products. We show that AIPOcean reduces the errors of subsurface temperature and salinity, and reproduces mesoscale eddies. In contrast to ECCO and SODA products, AIPOcean captures the interannual variability and linear trend of sea level anomalies very well. AIPOcean also shows a good consistency with tide gauges.

Key words: ocean data assimilation, reanalysis, ensemble optimal interpolation, background error covariance

Citation: Yan, C. X., J. Zhu, and J. P. Xie, 2015: An ocean data assimilation system in the Indian Ocean and West Pacific Ocean. *Adv. Atmos. Sci.*, **32**(11), 1460–1472, doi: 10.1007/s00376-015-4121-z.

1. Introduction

The area surrounded by the Indian Ocean and West Pacific Ocean is a key area influencing short-term climate variation (seasonal to interannual) over China. The air–sea interaction (e.g., the exchange of energy, momentum and water masses) in this area is an important factor leading to extreme weather or meteorological disasters in China. Although some types of observations are available in this area, their discontinuity in time and space is an obstacle to understanding and studying air–sea interactions. Developing an ocean data-assimilation system combining various types of observations with an ocean model to construct a long-term reanalysis product may provide an important dataset for improving the understanding of the ocean and air–sea interactions in this area.

Several ocean data assimilation systems on regional or global scales have been developed for operational ocean forecasting or reanalysis products. The China Ocean Reanalysis (CORA) used a three-dimensional variational (3DVAR) analysis scheme that considered multi-scale observations based on the Princeton Ocean Model with a generalized coordinate system (POMgcs) (Han et al., 2011). CORA is also an important reanalysis product in Chinese coastal and adjacent seas. Han et al. (2013) completed a global reanalysis product based on the CORA project. Xiao et al. (2008) developed a 3DVAR system combined with the recursive-filter method applied over the global ocean (Wang et al., 2012). The Bluelink system focused on the Australian region using an ensemble optimal interpolation (Oke et al., 2008). The Multivariate Ocean Variational Estimation system, based on 3DVAR with coupled temperature and salinity empirical orthogonal function modes, was developed in the northwestern Pacific (Fujii and Kamachi, 2003). Additionally, TOPAZ from Norway (http://topaz.nersc.no), FOAM from the United Kingdom (Martin et al., 2007), ECCO and SODA (http://www.ecco-group.org; Carton et al., 2000) focused on different regions.

This paper describes the components of an ocean data assimilation system in the Indian Ocean and West Pacific Ocean in detail, and evaluates the performance via a multi-year data assimilation experiment. Here, we only focus on the evaluation of the ocean data assimilation system and provide some hints on the potential application of this system in a better

* Corresponding author: YAN Changxiang
Email: ycxlasg@mail.iap.ac.cn

understanding of air–sea interactions in the joint region. In view of this, the structure of this paper is as follows. The model is described in section 2. The assimilation scheme, based on ensemble optimal interpolation (EnOI) is presented in section 3. The pretreatment of the various types of observations used for the assimilation and domain partitioning with lower computational cost are detailed in section 4. A simple assessment of the data assimilation through comparisons with independent observations and other reanalysis products (such as ECCO and SODA) is presented in section 5. Finally, a conclusion and discussion are presented in section 6.

2. Model

The Hybrid Coordinate Ocean Model (HYCOM), which was developed from the Miami Isopycnic Coordinate Ocean Model (Bleck et al., 1992), is used. It is a primitive equation model with a hybrid vertical coordinate that is isopycnic in the open, stratified ocean, and smoothly transfers to a z-coordinate or terrain-following sigma coordinate in the weakly stratified or shallow waters. The K-Profile Parameterization vertical mixing scheme is included in HYCOM.

The model domain spans the West Pacific and Indian oceans over (28°S–44°N, 30°–180°E), which is one-way nested in an external model domain of (51°S–62°N, 30°–291°E) (Fig. 1). The conformal mapping of Bentsen et al. (1999) is additionally included to generate the model horizontal grid. The model resolution is increased from 20 km at the equator to 28 km at the southern and northern boundary of the domain, while the outer domain resolution ranges from 39 km to 84 km. There are 22 vertical hybrid layers with reference densities from 18.00 kg m^{-3} to 27.84 kg m^{-3} and with uniform resolution of 2/3 in the upper 10 layers.

The 6-hourly fields from the ERA-Interim (ERA: European Centre for Medium-Range Weather Forecasts Reanalysis) dataset including temperature, dew point temperature, mean sea level pressure and wind are used to force the model. The precipitation data are taken from the climatology of Legates and Willmott (1990). The temperature and salinity are relaxed toward monthly climatologies from the Generalized Digital Environmental Model (Teague et al., 1990) with a timescale of 60 days at the surface and lateral boundaries.

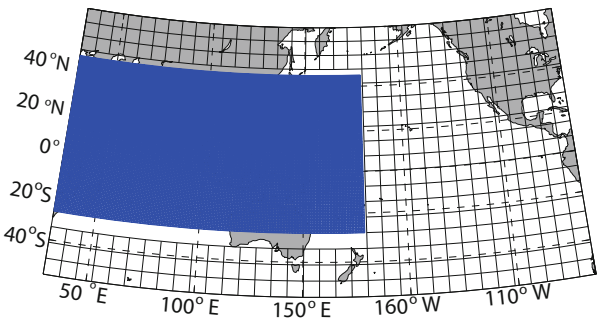

Fig. 1. The grid layout of the model. The blue grids are for the model domain, and the black for an external model domain. The meshes are drawn every three grids for the model domain, and every ten grids for the external domain.

3. Assimilation method

The EnOI (Evensen, 2003; Oke et al., 2008) is used in this study. The analysis is computed by solving the equation

$$\boldsymbol{\psi}_{\mathrm{a}} = \boldsymbol{\psi}_{\mathrm{b}} + \alpha(\boldsymbol{C}\circ\boldsymbol{P})\boldsymbol{H}^{\mathrm{T}}[\alpha\boldsymbol{H}(\boldsymbol{C}\circ\boldsymbol{P})\boldsymbol{H}^{\mathrm{T}} + \boldsymbol{R}]^{-1}(\boldsymbol{\psi}_{\mathrm{o}} - \boldsymbol{H}\boldsymbol{\psi}_{\mathrm{b}}) , \quad (1)$$

where $\boldsymbol{\psi} = (\boldsymbol{u},\boldsymbol{v},\boldsymbol{d},\boldsymbol{t},\boldsymbol{s},\boldsymbol{p}_{\mathrm{B}},\boldsymbol{u}_{\mathrm{B}},\boldsymbol{v}_{\mathrm{B}})$ is the state vector including baroclinic velocities, layer thickness, temperature, salinity, barotropic pressure, and barotropic velocities. The subscripts a, b, o and superscript T denote the analysis, background, observation and matrixei transpose respectively. $\boldsymbol{P}$ is the background error covariance matrix. $\boldsymbol{R}$ is the observation error covariance matrix. Since the relationship between the measurement errors is rarely estimated, the matrix $\boldsymbol{R}$ is usually considered as diagonal. $\boldsymbol{H}$ is the observation operator that interpolates from the model space to observation space. C is a localizing correlation function used to remove the effects of sampling error due to the ensemble size being smaller than the dimension of the model space. Each element of $\boldsymbol{C}$ is computed by a fifth-order piecewise rational function (Gaspari and Cohn, 1999) where the length scale is taken as 400 km. The localization function makes $\boldsymbol{P}$ equal to zero beyond the distance of the length scale. The circle between $\boldsymbol{C}$ and $\boldsymbol{P}$ denotes a Schur product. The parameter α is used to tune the magnitude of the covariance. Here, it is taken as 0.6.

The background error covariance matrix $\boldsymbol{P}$ is given by

$$\boldsymbol{P} = \frac{\boldsymbol{A}\boldsymbol{A}^{\mathrm{T}}}{(n-1)} ,$$

where $\boldsymbol{A}$ is a matrix consisting of n ensemble members, and is defined as $\boldsymbol{A} = (\boldsymbol{\psi}_1, \boldsymbol{\psi}_2, \cdots, \boldsymbol{\psi}_n)$. The ensemble members are taken from the model state anomalies and n is the ensemble size (120 in this study). It is clear that such an ensemble keeps the dynamical consistency between model variables. The EnOI usually uses a stationary ensemble of model states sampled during a long-term integration to estimate the structure of the background error covariances (Evensen, 2003). In the monsoon-dominated Indian Ocean, the sea surface current demonstrates seasonal differences. The structure of the background error covariances estimated by the stationary ensemble is not capable of reflecting the seasonal evolution of the sea surface current very well. In view of this, different ensembles in different seasons are adopted in this study. The ensemble $\boldsymbol{A}$ consists of anomaly data defined as the daily model state minus the monthly average over the 18-year model run. In each season, the ensemble with the size of 120 is randomly sampled from the anomaly dataset, which subsamples an anomaly every 9 days from the 18-year model integration in this season.

The EnOI code taken from the TOPAZ system (Bertino and Lisæter, 2008) is used to assimilate sea level anomalies and SST. In view of the isopycnic coordinate included in HYCOM, a different ensemble-based technique, that of Xie

and Zhu (2010), is used to assimilate *in-situ* temperature and salinity profiles. In this technique, the observed temperature and salinity profiles are firstly converted to layer thicknesses as "observations". Secondly, the layer thickness "observations" are assimilated to adjust the model layer thickness and model velocity fields. Finally, the observed temperature (or salinity) profiles are assimilated to adjust the model temperature (or salinity), followed by diagnosing the model salinity (or temperature) from the equation of seawater state. This technique ensures the linearity of observation operators. The straightforward method is to adjust the model variables by assimilating the temperature and salinity observations. This may lead to the strong nonlinearity of observation operators, and may cause serious problems.

Compared with the variational methods (such as 3DVAR), the EnOI has some apparent differences. For 3DVAR, the background error covariance matrix is usually estimated using the simplified correlation functions that exponentially decay the correlations with the increasing spatial distance. The EnOI uses an ensemble taken from the model simulations to estimate the background error covariance that may allow more anisotropic and inhomogeneous patterns. The EnOI tends to improve the model results in a moderate and tractable way, while the 3DVAR tends to somewhat intensify false changes due to the empirical-function-determined variances of background errors in the sea level anomaly (SLA) assimilation (Fu et al., 2009a).

4. Observations for assimilation

4.1. *Observation sources for assimilation*

The assimilated subsurface temperature and salinity observations are obtained from the Met Office quality controlled EN dataset, using version EN3 1d, which was the version available at the time the work was carried out (http://www.metoffice.gov.uk/hadobs/en3), available from 1950. This dataset consists of the World Ocean Database 2005, Global Temperature and Salinity Profile Project, Array for real-time geostrophic oceanography (ARGO), and the Arctic Synoptic Basin-wide Observations, and is updated online on a fast and regular basis. In this version of EN3, the XBT (expendable bathythermograph) bias correction of Wijffels et al. (2008) is applied. However, the ARGO biases due to the drift of the pressure sensors are not corrected. As addressed by Willis et al. (2009), the ARGO biases may cause false signals. Therefore, it is necessary to carry out quality control on ARGO observations before the assimilation. We remove all suspected ARGO profiles included in the ARGO grey list by the CSIRO (Commonwealth Scientific and Industrial Research Organisation) website. A large number of questionable ARGO profiles cover almost all of the global ocean. If these profiles are assimilated into the model, the negative effects are not negligible (Yan and Zhu, 2010).

Since the geoid is not well known, the sea surface height cannot be used directly. In order to eliminate the uncertainty, the SLA relative to the time average is used for scientific studies. In this study, the mean dynamical topography calculated as a time average of the model sea surface height over 1993–1999 is added to the observed SLA for the comparisons with the model counterpart. The assimilated altimetry data are the global, merged SLA from all altimeters: Jason-2, Jason-1, Topex/Poseidon, Envisat, GFO, ERS-1/2 and Geosat. The multi-mission data are processed by the Data Unification and Altimeter Combination System developed by Collecte Localisation Satellite (CLS), to produce the merged SLA data, which are obtained by subtracting a time average of sea level measurement over the period 1993–1999. In this study, the merged SLA on a $(1/3)^\circ$ Mercator projection grid with a temporal resolution of 7 days from January 1993 to December 2006 is adopted. At each grid bin, the value represents the difference from the 7-year average. More details can be found in previous studies (Le Traon et al., 1998; Ducet et al., 2000).

The satellite-derived SST (Reynolds et al., 2007) is used for assimilation. This is generated using satellite SST data from the Advanced Very High Resolution Radiometer and Advanced Microwave Scanning Radiometer, and *in-situ* data from ships and buoys via the optimum interpolation method. Additionally, in view of the sparseness of *in-situ* data, a bias correction of the satellite data with respect to *in-situ* data is also made, using an empirical orthogonal teleconnection algorithm. The SST product has a spatial grid resolution of $(1/4)^\circ$ and a temporal resolution of 1 day with global coverage. A more detailed description of this product can be found in Reynolds et al. (2007).

4.2. *Pretreatment of observations*

According to the analysis equation, Eq. (1), a large matrix needs to be stored and inverted. In practice, this is not feasible, particularly for high-density observation areas. One feasible technique to solve this problem is super-observation. This method has been widely used for data assimilation (Cummings, 2005; Salonen et al., 2009) and for remote sensing data to remove random observation errors (Seko et al., 2004). A so-called super-observation is a spatial average with a smaller error over a small number of observations with known errors. In the data assimilation, there is a one-to-one matching between the observed quantity and the model counterpart in a grid cell. If the number of observations is very large, more than one observation may fall within a grid bin. These observations can possibly detect information that is not resolved due to the imperfectness of the numerical model, or represent the same information. The super-observations may filter some noise or eliminate redundant information relative to the model.

In this study, a super-observation is produced by a simple weighted average over all observations in every 2×2 model grid bin. By applying super-observations, the number of assimilated SLA observations may be greatly reduced from about 70 000 to 20 000. The computational demand is also greatly reduced.

For SST observations, a different observation-thinning scheme of Li et al. (2010) is adopted. This scheme can pick out a subset of observations with a small analysis error vari-

ance while keeping the observations as few as possible. With this scheme, the optimal observation locations used in data assimilation are identified. Moreover, the observation density is thinned by about 95%. This means only 5% of SST observations are assimilated. The computational cost is not expensive.

For *in-situ* temperature and salinity profiles, a different scheme is used for thinning. Different profiles have different vertical levels. Calculating the horizontal average over profiles presents some problems. Using a method similar to that of Oke et al. (2008), we select a good profile from the profile observations falling in each 2×2 model grid bin, rather than take an average. The selection order is as follows: first an ARGO profile, then CTD (conductivity–temperature–depth), then TAO (Tropical Atmosphere Ocean Project), and finally XBT/MBT (MBT: mechanical bathythermograph).

In order to better constrain the analysis with more observations, a 7-day window is used to assimilate temperature and salinity profiles. The different weightings are imposed on the observations based on the time distance from the assimilated moment. SLAs and SST with approximate global coverage are assimilated once every seven days.

4.3. *Domain partition*

Different types of observations have different temporal and spatial distribution features. The remotely sensed data provide approximate homogeneous cover. The distribution of temperature and salinity observations is extremely irregular (Fig. 2), especially before the ARGO era. It can be seen that the high-density profiles are concentrated in the vicinity of Japan. In this study, the localization is performed at each model gridpoint in the same way as Evensen (2003). Therefore, more observations are available within the radius of correlation scale for a given point in the profile-dense regions. The resultant large matrix makes the inversion expensive at every gridpoint. Moreover, the computation is very time-consuming. For example, when using 192 000 horizontal gridpoints with 5600 gridpoints near Japan, the computational time of assimilating in a single step is 72 hours. According to this efficiency, a 1-year assimilation experiment with an assimilation frequency of four in every month will last 144 days. That is extremely expensive.

The domain partition technique is one approach to deal with this issue. Oke et al. (2008) divided the global domain into about 800 sub-domains. Fu et al. (2009b) divided the global ocean into three ocean basin domains. In this study, a domain-partition method based on the model grid cells is attempted. Every 5×5 model grid cell is regarded as a sub-domain. In each sub-domain, the assimilation is carried out locally and is seamless and continuous between adjoining sub-domains. The approach is more suitable to the assimilation of irregular observations, and with high computational efficiency. By application to the above instance, the time consumed in a single assimilation is reduced to 2 hours.

5. Results

In this section, we assess the data assimilation system by comparing with a free-run experiment without data assimilation, and with reanalysis products such as ECCO and SODA. Moreover, independent observations such as surface drifters, observed current fields, tide gauges, and withdrawn temperature and salinity profiles are further examined to assess the performance.

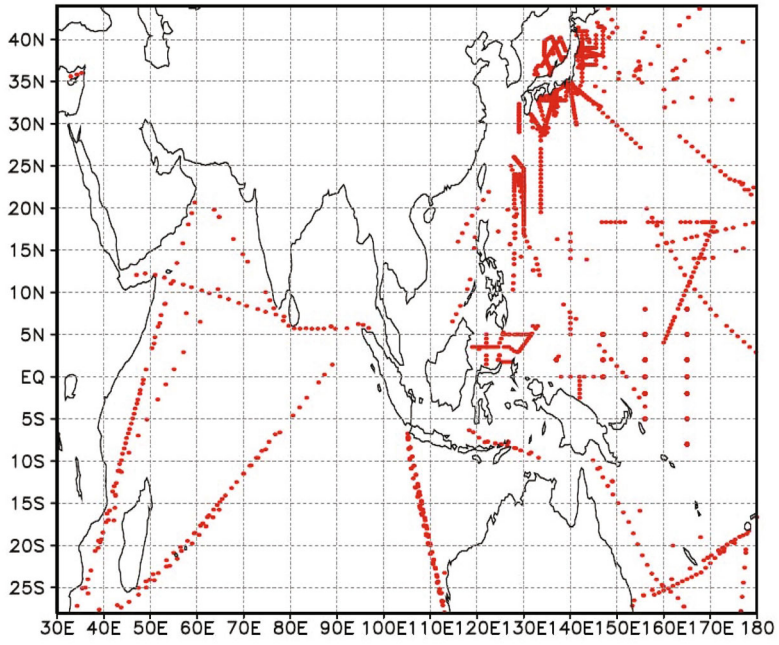

Fig. 2. The distribution of *in-situ* temperature observations in February 1999.

A long-duration (1992–2006) data assimilation experiment is carried out in the Indian and West Pacific oceans (hereinafter referred to as AIPOcean), combining temperature and salinity profiles from XBT, TAO (McPhaden et al., 1998), CTD and ARGO, remotely-sensed SST, and altimetry SLA data with the HYCOM model by the EnOI. The multi-year free-run experiment with no data assimilation is performed to provide an ensemble member for estimation of the background error covariance matrix, and also to be used for evaluating the assimilation system.

5.1. *Comparison with independent in-situ temperature and salinity profiles*

Not all ARGO profiles are assimilated in the HYCOM. A fraction of ARGO profiles withheld from the assimilated data are used to validate the performance. In the studied domain, more than 5000 ARGO profiles are not assimilated in the period 2004–2006 (Figs. 3a and b). The withheld observations are mostly distributed in the open sea, while in some coastal regions, such as the China Sea and Indonesian Throughflow, they are very sparse (Figs. 3a and b). The root-mean-square error (RMSE) of AIPOcean is consistently less than the RMSE of the free-run (Figs. 3d–g). This indicates an advantage of the assimilation method. However, there is an obvious temperature difference between AIPOcean and the World Ocean Atlas (WOA05), especially in the thermocline (Fig. 3d). The possible reason for the difference is as follows. The RMSEs are very sensitive to the accuracy in the locations of mesoscale eddies, meanders and fronts. For example, if an eddy is misplaced, the magnitude of the errors may be increased greatly. Therefore, the climatological estimate including no eddies has a smaller RMSE than an estimate from the reanalysis containing eddies that are in the wrong place (Oke et al., 2008). In the western Pacific, the RMSE of AIPOcean is slightly greater than the RMSE of WOA05 (Fig. 3f). This indicates that the large difference comes from the Indian Ocean, and is possibly associated with the model configuration (such as the parameterization scheme, vertical

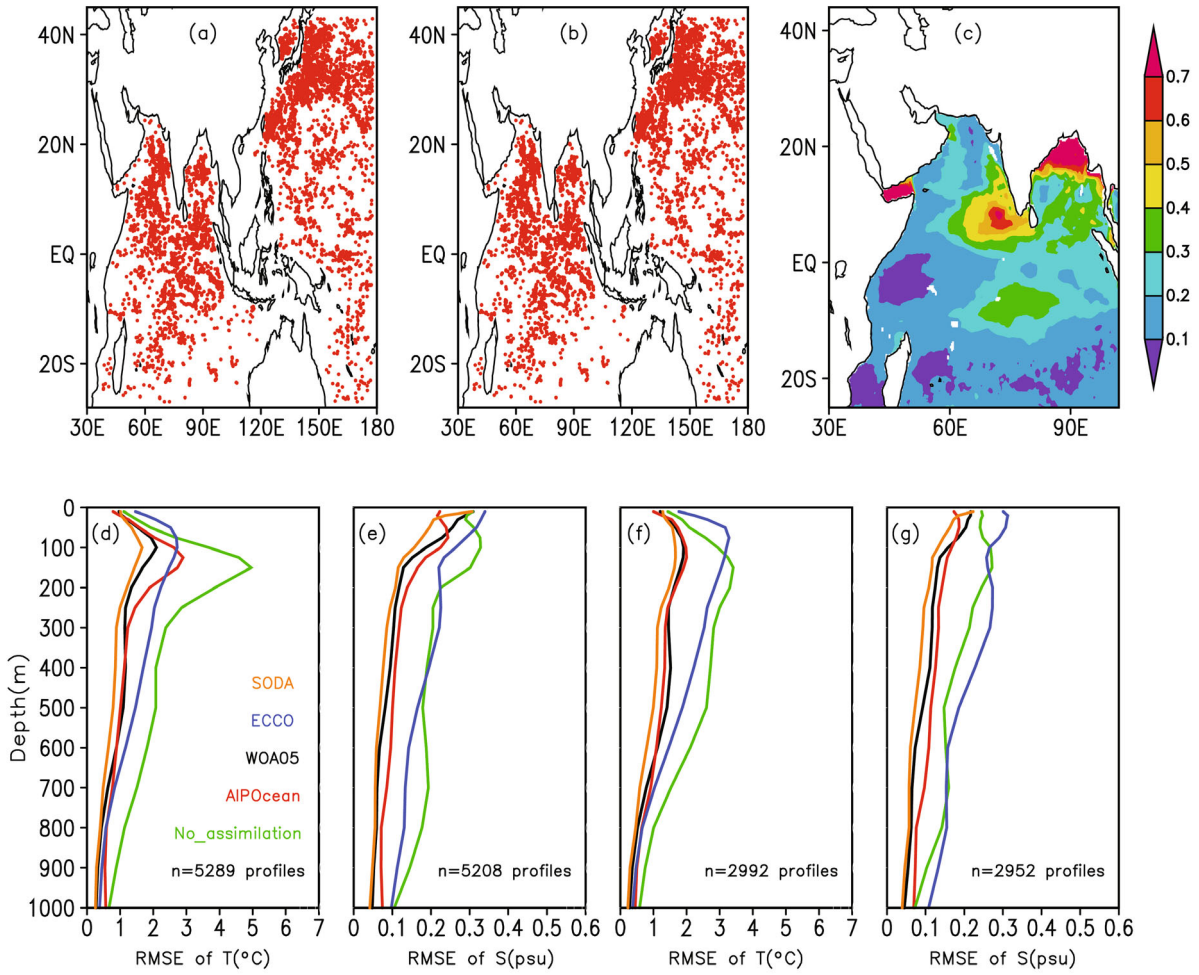

Fig. 3. The distribution of (a) temperature and (b) salinity observations withheld from the data assimilation during the period of 2004–2006, and depth profiles of the RMSEs of (d, f) temperature and (e, g) salinity, relative to the independent ARGO observations from the free run without data assimilation (blue), AIPOcean (red), climatology data WOA05 (black), ECCO (blue), and SODA (orange) in the (d, e) model domain and (f, g) western Pacific, and (c) the variability (units: psu) of sea surface salinity relative to the period of 2004–2006.

resolution etc.). The large temperature gradient in the thermocline needs a fine vertical resolution. The vertical parameterization scheme may affect the vertical mixing, and the vertical stratification. In our study, the performance of the model is not very good in the thermocline (Fig. 3: the experiment without data assimilation). For the salinity in the near surface, the RMSE of AIPOcean is significantly less than the RMSE of WOA05 in the whole domain (Fig. 3e). This mainly comes from the positive contribution of the Indian Ocean because the RMSE of AIPOcean is slightly less than that of WOA05 in the western Pacific (Fig. 3g). The interannual variabilities of sea surface salinity (SSS) from AIPOcean in the Bay of Bengal and Arabian Sea are much greater for the period of 2004–2006 (Fig. 3c). The interannual signals are lacking in the climatology of WOA05, which may partly demonstrate why the AIPOcean SSS is better than that of WOA05. Additionally, we calculate the RMSEs of ECCO and SODA using the monthly mean data related to the same observations. It is very clear the RMSE of ECCO is typically greater than that of the WOA05 climatology for both temperature and salinity profiles. SODA shows the best results with the lowest RMSEs. Possibly, the observations used for calculating RMSE were assimilated in SODA, which would reduce the RMSE, and the performance of SODA is possibly better for temperature and salinity assimilation.

5.2. *Comparison with independent current observations*

Surface velocity measurements are much more scarce compared with temperature and salinity observations. However, the coverage of surface velocity measurements is greatly improved by the global drifter program. Since no velocity observations are assimilated in the AIPOcean reanalysis, drifters provide an independent dataset to validate the reanalysis. The drifter data collected and processed by the Atlantic Oceanographic and Meteorological Laboratory under the global drifter program, formerly the World Ocean Circulation Experiment–Surface Velocity Programme, are used in this study.

Figure 4 shows the distribution of the monthly sea surface current from the AIPOcean in November 2006 superimposed by the trace of drifters in the Indian Ocean. The drifters with trajectories longer than 10 days in November 2006 are used for comparison. The red points denote the start locations of the drifters. The characteristics of the sea surface current can be seen (such as eddies, eastern current, western boundary current, etc.). In the Bay of Bengal, an anticyclonic eddy is clearly present in the AIPOcean (Fig. 4b), which is traced by drifter B4. The AIPOcean also shows good agreement with other drifters. In the Arabian sea, the drifters basically trace the ocean circulation of the AIPOcean closely (Fig. 4a). This implies that the AIPOcean has a certain potential for capturing the eddies and reproducing the features of the circulation in the northern Indian Ocean.

Additionally, the velocity measurements from moored ocean buoys of the TAO project are also used for validation. Since reanalysis products such as ECCO, SODA and AIPOcean are monthly, the monthly TAO data are used for comparison.

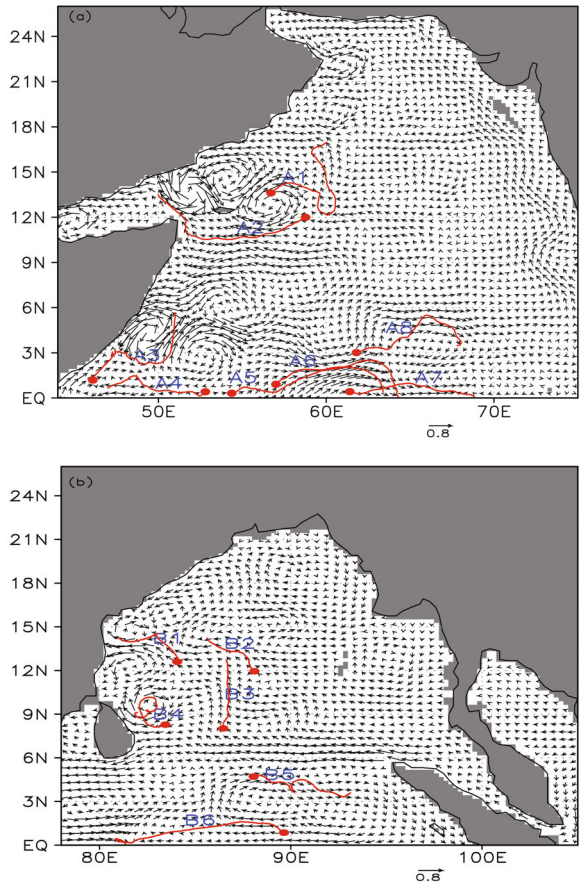

Fig. 4. The monthly sea surface current and trajectories (red) of surface drifters in the northern Indian Ocean including the Arabian sea (a) and the Bengal bay (b) in November 2006. The drifters with trajectories longer than 10 days in November 2006 are used. The red points denote the start positions of drifters as follows: A1 (13.6°N, 56.7°E), A2 (12°N, 58.7°E), A3 (1.2°N, 46.1°E), A4 (0.4°N, 52.8°E), A5 (0.3°N, 54.4°E), A6 (0.9°N, 57°E), A7 (0.4°N, 61.4°E), A8 (3°N, 61.8°E), B1 (12.6°N, 84.1°E), B2 (11.9°N, 88.1°E), B3 (8°N, 86.5°E), B4 (8.3°N, 83.4°E), B5 (4.7°N, 88.1°E), B6 (0.8°N, 89.6°E).

Figures 5a and c show the evolution of a zonal current and zonal current difference at the sea surface at the location (2°S, 156°E). It is very clear that the model simulations without data assimilation and all reanalysis products capture the interannual variability of sea surface current, and show a similar pattern to observations. This is also indicated by strong correlations between reanalysis datasets and observations. AIPOcean basically shows small differences from observations. Moreover, the AIPOcean reanalysis is closer to the Research moored Array for Afican–Asian–Australian Monsoon Analysis and prediction (RAMA; McPhaden et al., 2009) data than other products in terms of the RMSEs and correlations. For a location in the Indian Ocean [(1.5°S, 90°E); Figs. 5b and d), the AIPOcean reanalysis is strongly correlated with observations. The consistency between the AIPOcean reanalysis and RAMA is better. The correlation coefficient reaches 0.8, while it is slightly smaller for the

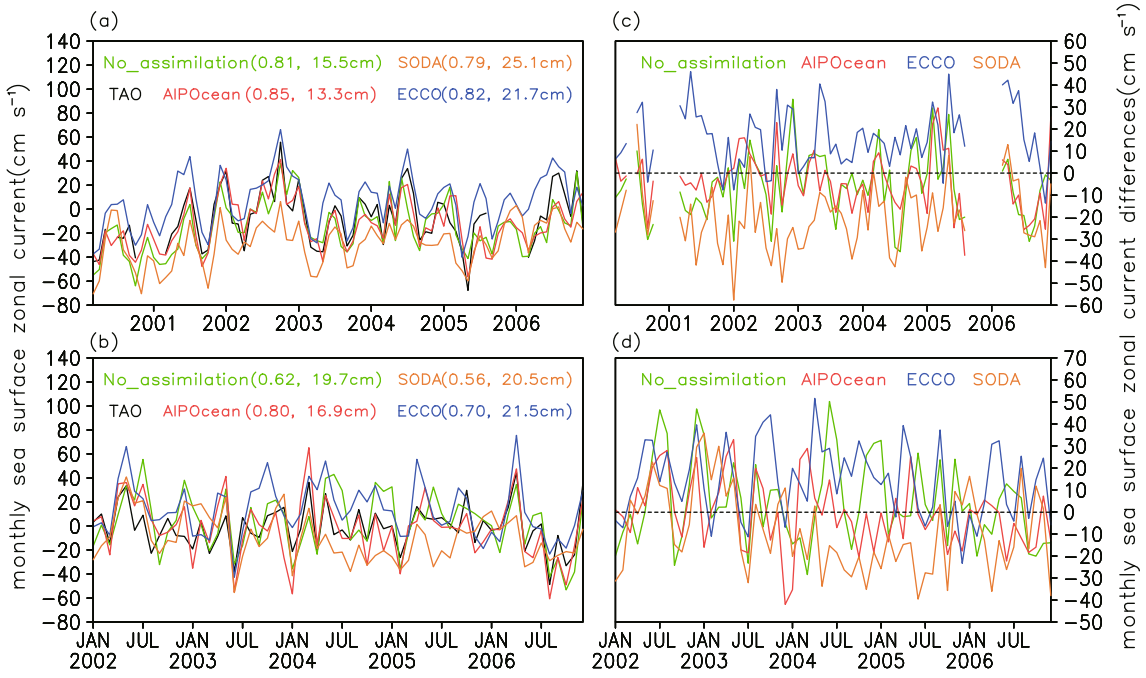

Fig. 5. Monthly sea surface zonal current (left) (units: cm s^{-1}) from TAO (black), No_assimilation (green), AIPOcean (red), ECCO (blue), and SODA (orange) and the differences (right) (units: cm s^{-1}) between the products and TAO observations at the location of (a, c) (2°S, 156°E) and (b, d) (90°E, 1.5°S). The numbers in brackets indicate the correlation between the reanalysis and TAO observations and the RMSE of reanalysis, respectively.

other two products. Moreover, the RMSE of the AIPOcean reanalysis is the lowest. The improvement over the experiment without assimilation is also very clear.

The Indonesian seas provide a series of complex passages linking the Pacific and Indian oceans. The Indonesian Throughflow (ITF), which transports water from the tropical Pacific Ocean to the Indian Ocean through the Indonesian seas, is an interoceanic exchange process. The ITF has been shown to play an important role in the thermocline-driven global circulation system (Gordon, 1986). Some studies have also shown a significant influence of the ITF on the global air–sea system via ocean general circulation models or coupled climate models (Hirst and Godfrey, 1993; Schneider and Barnett, 1997; Schneider, 1998; Banks, 2000; Wajsowicz and Schneider, 2001; Lee et al., 2002; Pandey et al., 2007). In this subsection, the ITF transport of the AIPOcean reanalysis is evaluated.

The Indonesian water is exported to the Indian Ocean via three main passages: the Lombok Strait, Ombai Strait and Timor Passage; and is imported from the Pacific Ocean by the Makassar Strait, Lifamatola Passage and other straits (e.g. the Karimata Strait, Torres Strait etc.). For a consistent comparison with observations from the INSTANT program (Gordon et al., 2009), the 3-year mean inflow transport is calculated as the sum of the Makassar Strait and Lifamatola Passage inflows, while outflow is calculated as the sum of the Lombok Strait, Ombai Strait and Timor Passage outflows. The INSTANT program observed a 3-year net outflow of 15 Sv, and an inflow of 12.7 Sv (Table 1). The ITF transports from the three reanalyses (AIPOcean, ECCO and SODA) are overall lower than the observations. For the inflow, SODA yields 8.2 Sv, which is much lower than observations, while AIPOcean and ECCO show 11.9 Sv and 10.2 Sv, respectively. For the outflow, ECCO presents the lowest transport of 11.7 Sv, while AIPOcean and SODA present similar magnitudes greater than 14 Sv. The AIPOcean shows a better 3-year net ITF transport than ECCO and SODA. The difference in ITF transports may be related to the resolution and topography of different reanalyses in the Indonesian passages.

5.3. *Comparison with observed SLAs*

The monthly averaged data from different products are used to compute the standard variance of sea level over the 14-year period of 1993–2006 (Fig. 6). As a comparison, the experiment with a horizontal resolution of $1° \times 1°$ using the EnOI method and HYCOM is also carried out (hereafter referred to as Exp1 $\times$ 1). The altimetry data show strong

Table 1. The three-year mean Indonesian Throughflow transport in Sv (10^6 m^3 s^{-1}) during 2004–2006.

	Annual mean inflow (2004–2006)	Annual mean outflow (2004–2006)
Observation (Gordon et al. 2009)	12.7 Sv	15 Sv
AIPOcean	11.9 Sv	14.5 Sv
ECCO	10.2 Sv	11.7 Sv
SODA	8.2 Sv	14.2 Sv

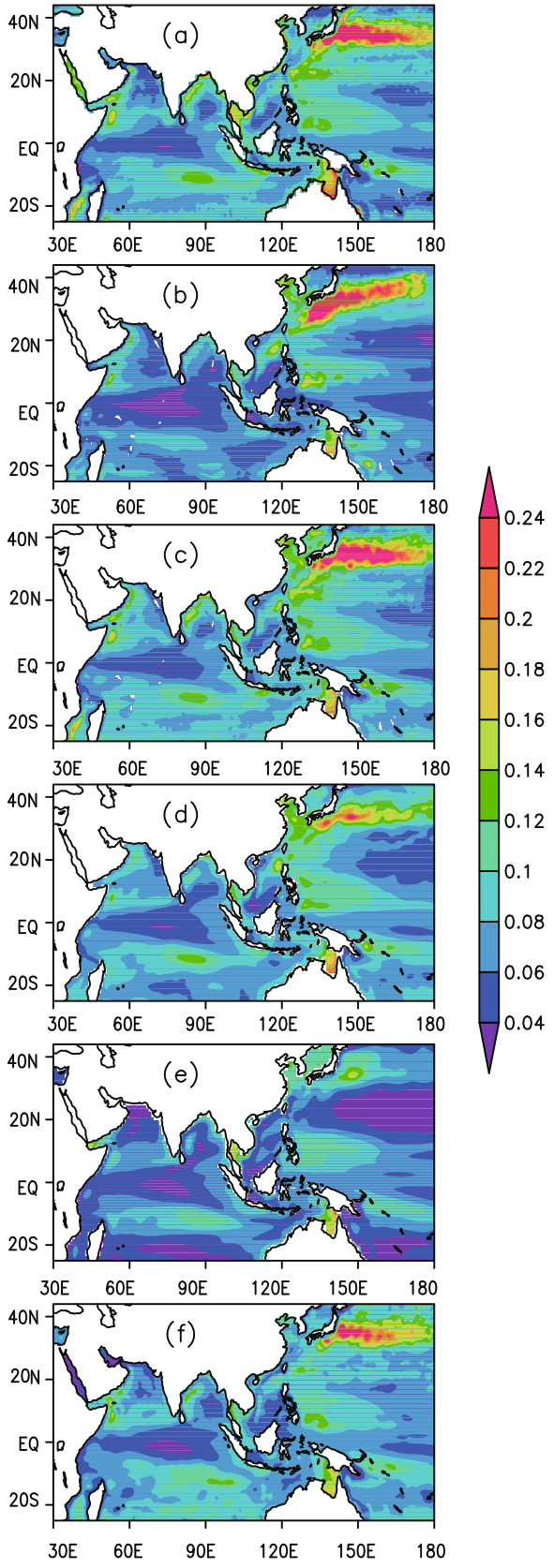

Fig. 6. The variability (units: m) of monthly sea level anomalies during the period 1993–2006 from (a) observations, (b) No_assimilation, (c) AIPOcean, (d) Exp1x1, (e) ECCO and (f) SODA.

signals of sea level variability greater than 20 cm in a zonal band east of Japan in the northwestern Pacific. The large variability is related to the plentiful eddies in this region. Additionally, large variation can also occur in some regions of western boundary currents and in the coastal regions. Some large variabilities show a correspondence with large current systems. For example, the region of large variation corresponds to the Kuroshio Current in the West Pacific.

The experiment without assimilation can capture the strong signals in the northwestern Pacific. However, the large-variability area extends from the south of Japan to the northeast. The path seems inconsistent with the observations. This is possibly related to the Kuroshio extension simulated by the model. The AIPOcean reanalysis reproduces strong variability and demonstrates a good agreement with observations. In the northwestern Pacific, the Exp1 $\times$ 1 also captures some signals. Moreover, the zonal band with large variabilities is similar to observations. The signals concerned with eddies are relatively weak. Overall, the pattern of variabilities from the Exp1 $\times$ 1 is consistent with observations. The pattern of sea level variability for SODA, with a resolution of $0.25^\circ \times 0.4^\circ$ in zonal and meridional directions, is similar to observations, but the magnitudes are weaker than those for AIPOcean. ECCO greatly underestimates the standard variance of sea level, meaning it misses the strongest variability peak compared with the altimetry data. Since the resolution of ECCO is relatively coarse at $1^\circ \times 1^\circ$, enhanced to $(1/3)^\circ$ in the north–south direction within 10° of the equator in the northwestern Pacific, some mesoscale eddies are not resolved well. As a result, the variability signal concerned with eddy development, especially in the northwestern Pacific, is not captured well. The resolution is one of the important factors affecting the variability. Additionally, the assimilation of the high-resolution SLA also plays a certain role. The AIPOcean reanalysis does have an advantage over the other two products in terms of resolution. Compared with Exp1 $\times$ 1, the variabilities of ECCO are low throughout the domain, despite relatively high resolution in the equatorial ocean. This is possibly related to the assimilation method used.

Additionally, we compare the linear trend in sea level over the past 14 years from the observations and each of the reanalysis products (Fig. 7). The distribution of the trend in sea level is not spatially uniform. During the past 14 years, the western Pacific south of 30°N and the south Indian Ocean basically show an increase in sea level. The band of 30°–40°N presents both strongly decreasing and increasing trends. These complicated phenomena are associated with the Kuroshio Current extension and nearby active eddies. For the experiment without assimilation, a significant rise in sea level is shown in some zonal bands of the western Pacific. For the AIPOcean reanalysis, the obvious trend is concentrated in the western Pacific, and is very similar to the spatial distribution of observations. ECCO shows a rise in sea level throughout the western Pacific. The zonal band of a mixture of increased and decreased sea level cannot be found. SODA shows a notable decrease to the south of 18°S, different from the altimetry data. Additionally, in the zonal band of 18°–

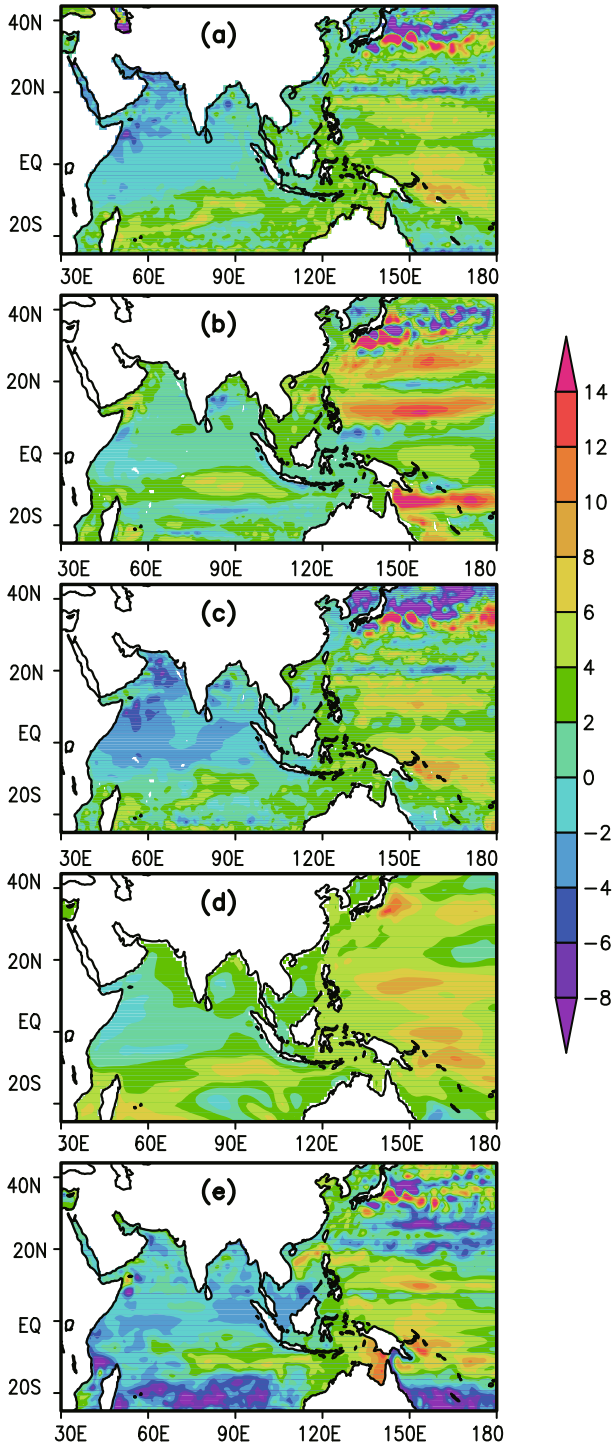

Fig. 7. The linear trend (units: mm yr^{-1}) of monthly sea level anomalies during the period 1993–2006 from (a) observations, (b) No_assimilation, (c) AIPOcean, (d) ECCO and (e) SODA.

30°N, an opposite trend to the observations is also demonstrated.

To further evaluate the AIPOcean reanalysis, we compare it with the independent tide gauge dataset processed by the University of Hawaii Sea Level Center. In this study, we examine the dataset to identify stations with a time span of no less than 10 years, located in the model domain, and situated within four different model ocean grids. According to these criteria, 57 gauges are available. At each station, the correlation between the annual AIPOcean reanalysis and tide gauge sea level is calculated (Table 2). To discard the effect of sea level rise due to model biases, land ice-melt, and other factors unresolved by the ocean model, we remove the linear trend from the annual sea level data. The gauge and AIPOcean reanalysis sea level data show correlation greater than 0.8 at 43 stations. A correlation below 0.7 is found only for one station. The average correlation over all stations is 0.87. Moreover, the correlations of gauge and AIPOcean reanalysis sea level data in almost all stations exceed the 99% level of statistical significance, except for two stations with a 98% significance level.

The comparison of time series at three stations shows good agreement between AIPOcean reanalysis and observed sea level (Fig. 8). The high and low sea level events in the time series reflect the effects of El Niño in the western tropical Pacific. The strongest event in the studied period is the 1997–1998 El Niño event, which corresponds to a decrease in sea level. Moreover, the AIPOcean reanalysis demonstrates consistent interannual signals with observed sea level. Compared with the experiment without assimilation, ECCO and SODA, the AIPOcean also shows the best results, as implied by the reduced RMSE and the high correlation with observa tions. Moreover, the magnitude of the difference between AIPOcean and tide gauge data is relatively small.

6. Discussion and conclusions

A data assimilation system generating an AIPOcean reanalysis in the Indian Ocean and western Pacific Ocean has been described in detail. The thinning of observations (superobserving) and domain partitioning for lower computational cost have been presented. The EnOI method is used to assimilate various types of observations. However, for temperature and salinity profiles, a different scheme is used to assimilate layer thickness observations, calculated from observed temperature and salinity profiles, to adjust the model layer thickness and current fields, and then to assimilate temperature or salinity observations to adjust the model temperature or salinity, followed by diagnosing the model salinity or temperature.

We evaluated the data assimilation system through a series of qualitative and quantitative comparisons between AIPOcean and other reanalysis products, satellite data, independent temperature and salinity observations, observed current fields, surface drifters, and tide gauges. Through these comparisons, we have shown that AIPOcean reconstructs the basin-scale ocean circulation and mesoscale eddies. The subsurface temperature and salinity from AIPOcean are typically improved, especially at the thermocline in the Indian Ocean and western Pacific Ocean. Surface zonal currents capture seasonal or interannual variabilities with strong correlations with observations and reduced RMSEs in comparison to other reanalyses. The sea level data show good agreement with tide

Table 2. Correlations between AIPOcean and tide gauge sea level at different stations.

No.	Station name	Location	Years	Correlation
1	Betio	1°22′N, 172°56′E	14	0.97
2	Majuro	7°6′N, 171°22′E	14	0.95
3	Malakal	7°20′N, 134°28′E	14	0.99
4	Yap	9°31′N, 138°8′E	14	0.96
5	Honiara	9°26′S, 159°57′E	13	0.98
6	Saipan	15°14′N, 145°45′E	13	0.95
7	Kapingam	1°6′N, 154°47′E	14	0.91
8	Port vil	17°46′S, 168°18′E	14	0.94
9	Chichiji	27°6′N, 142°11′E	14	0.89
10	Minamito	24°18′N, 153°58′E	10	0.79
11	Wake isl	19°17′N, 166°37′E	14	0.91
12	Guam	13°26′N, 144°39′E	13	0.96
13	Kwajalei	8°44′N, 167°44′E	14	0.95
14	Mombasa	4°4′S, 39°39′E	12	0.82
15	Port lou	20°9′S, 57°30′E	14	0.78
16	Rodrigue	19°40′S, 63°25′E	14	0.83
17	Gan	0°41′S, 73°9′E	14	0.92
18	Point la	4°40′S, 55°32′E	14	0.88
19	Langkawi	6°26′N, 99°46′E	14	0.95
20	Tapha	7°50′N, 98°26′E	14	0.76
21	LAMU	2°16′S, 40°54′E	12	0.9
22	Zanzibar	6°9′S, 39°11′E	14	0.92
23	Carnarvo	24°53′S, 113°37′E	13	0.99
24	Cocos is	12°7′S–96°54′E	14	0.75
25	Booby is	10°36′S, 141°55′E	14	0.83
26	Nakano s	29°50′N, 129°51′E	14	0.9
27	Abashiri	44°1′N, 144°17′E	14	0.87
28	Aburatsu	31°34′N, 131°25′E	14	0.78
29	Naha	26°13′N, 127°40′E	14	0.78
30	Maisaka	34°41′N, 137°37′E	14	0.79
31	Nase	28°23′N, 129°30′E	14	0.83
32	Nagasaki	32°44′N, 129°52′E	14	0.75
33	Nishinoo	30°44′N, 131°E	14	0.84
34	Ishigaki	24°20′N, 124°9′E	14	0.77
35	Lombrum	2°2′S, 147°22′E	13	0.97
36	Lautoka	17°36′S, 177°26′E	14	0.79
37	Tanjong	1°16′N, 103°51′E	14	0.77
38	Hiron Point	21°47′N, 89°28′E	11	0.8
39	Coxs Bazaar	21°27′N, 91°50′E	11	0.7
40	Kelang	3°3′N, 101°22′E	14	0.97
41	Keling	2°13′N, 102°9′E	14	0.96
42	Lumut	4°14′N, 100°37′E	14	0.95
43	Penang	5°25′N, 100°21′E	14	0.97
44	Funafuti-B	8°30′S, 179°13′E	14	0.96
45	Cendering	5°16′N, 103°11′E	14	0.87
46	Johor Baharu	1°28′N, 103°48′E	14	0.85
47	Kuantan	3°59′N, 103°26′E	14	0.88
48	Tioman	2°48′N, 104°8′E	14	0.91
49	Sedili	1°56′N, 104°7′E	14	0.83
50	Kukup	1°20′N, 103°27′E	14	0.9
51	Geting	6°14′N, 102°6′E	14	0.86
52	Kaohsiung	22°37′N, 120°17′E	14	0.63
53	Keelung	25°9′N, 121°45′E	12	0.92
54	Miyakejima	34°4′N, 139°29′E	11	0.75
55	Legaspi	13°9′N, 123°45′E	12	0.95
56	Bintulu	3°13′N, 113°4′E	13	0.86
57	Sandakan	5°49′N, 118°4′E	13	0.96

gauges. The AIPOcean captures the variability signals and linear trend of sea level anomalies very well, in comparison with ECCO and SODA. The analysis differences are partly associated with the resolution of the models, and also with the assimilation of high-resolution SLA observations. For SODA and ECCO, relatively coarse-resolution SLA observations are used for assimilation.

These comparisons demonstrate the performance of this data assimilation system. The performance could be improved when the new version of EN4 data are assimilated, and the configurations of the model are redesigned. Data from AIPOcean, including daily three-dimensional temperature, salinity, and current fields, as well as sea surface height, is freely available from the Information Center of the Institute of Atmospheric Physics (http://dell2.iap.ac.cn/index.php/component/mtree/142). Such data have been used to study the evolution of mesoscale eddies (Zu et al., 2013). The tropical cyclones (typhoons) formed in the tropical oceans are an example of extreme air–sea interaction, and the energy of these typhoons is mainly supplied by the ocean through sea surface fluxes (Emanuel, 1986). The impacts of mesoscale eddies on typhoons are not negligible. Both warm eddies and cold eddies may rapidly impact typhoon intensities (Emanuel, 1999; Shay et al., 2000; Lin et al., 2005; Walker et al., 2005; Wu et al., 2007; Zheng et al., 2008; Lin et al., 2009; Jaimes and Shay, 2009; Zheng et al., 2010; Walker et al., 2014). Warm eddies help to maintain and even intensify typhoons by serving as an insulator against the negative feedback of the ocean (Lin et al., 2005). Cold eddies can induce a rapid weakening of typhoons by the decrease in the translation speed and SST cooling (Walker et al., 2014). Compared with other reanalysis products, AIPOcean shows better performance in capturing mesoscale eddies, particularly in the western North Pacific, which contains many eddies and frequent passages of typhoons. This suggests that AIPOcean data have the potential for improving understanding of typhoon–eddy interactions, which is very important for improving typhoon intensity predictions. Additionally, the ITF, as a connection between the Indian Ocean and Pacific Ocean, can affect the latent heating over the Indian Ocean either by warming the ocean or by changing the ocean circulation (Godfrey and Weaver, 1991; Wajsowicz and Schopf, 2001; Wajsowicz, 2002). Moreover, latent heating is dominant among the components of the net surface heat flux in the Indian Ocean. Wajsowicz and Schopf (2001) showed that a change of 4 Sv in the mean ITF induced net surface heat flux differences of about 10 W m^{-2} in the region to the northeast of Madagascar and in a band near the west Australian coast. Furthermore, large evaporation rates occurred and were sustained in the southern Indian Ocean from 10°S to 30°S due to the heat supplied by the ITF in boreal summer. The resultant abundant water vapor in the atmosphere was carried northward across the equator by the summer monsoon. The moisture supply from the southern Indian Ocean fueled the rainfall. Thus, the strength of the Indian monsoon measured by rainfall during the southwest monsoon may be affected by the ITF. For the ITF, AIPOcean presents a similar magnitude

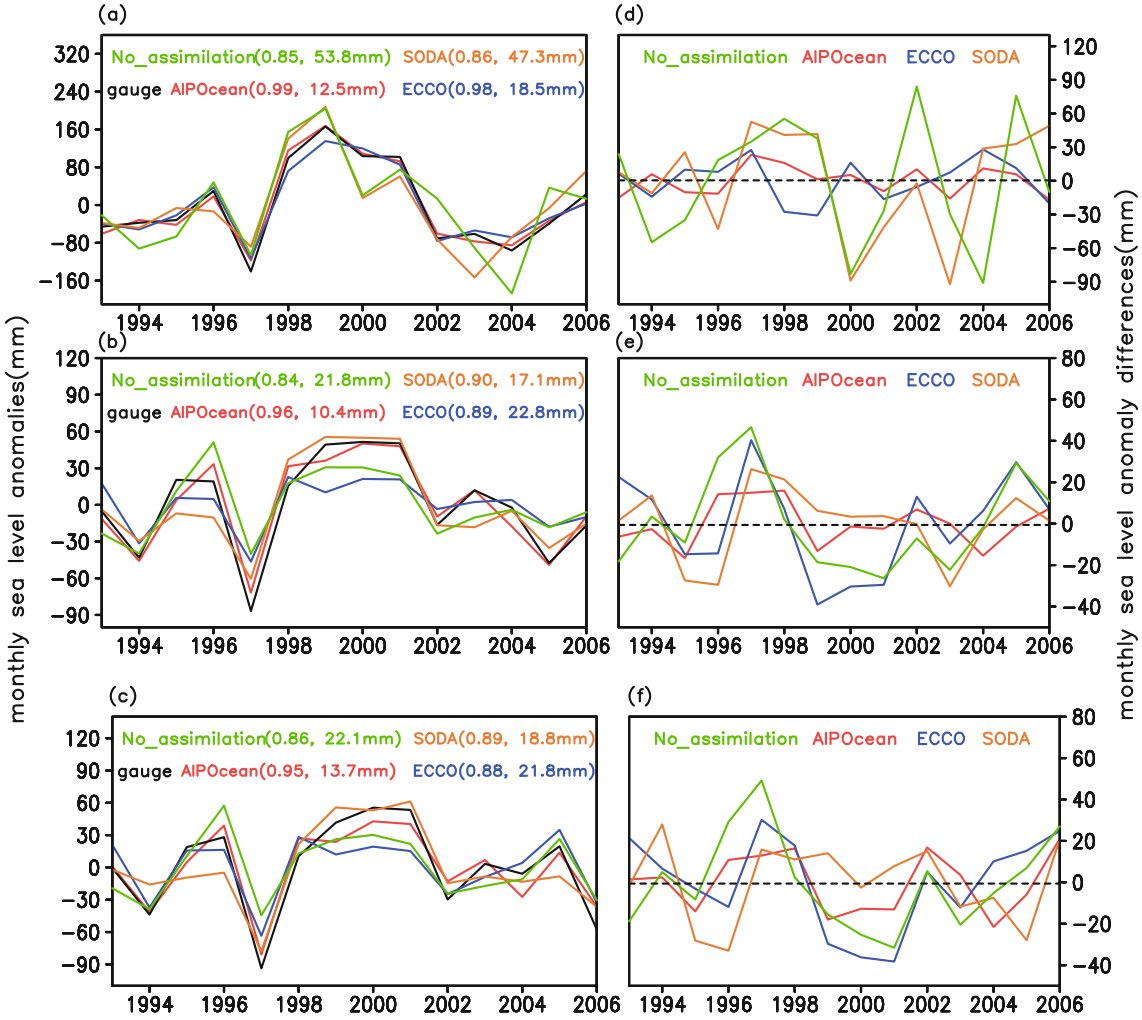

Fig. 8. Monthly sea level anomalies (left) (units: mm) removing the linear trend from tide gauge (black), No_assimilation (green), AIPOcean (red), ECCO (blue), and SODA (orange), and the differences (right) (units: mm) between products and tide gauge observations at different stations: (a, d) (7.3°N, 134.5°E); (b, e) (2.2°N, 102.1°E); (c, f) (6.4°N, 99.7°E). The numbers in brackets indicate the correlation between the reanalysis and TAO observations and the RMSE of reanalysis, respectively.

of the transport to observations, compared with other reanalysis products. Moreover, resolution can affect the impact of the ITF on the Indian Ocean: for a coarse-resolution system the signatures of the ITF in the mixed layer and themocline can be lost or diluted soon after entering the Indian Ocean; while for a fine-resolution system, there is little loss in heat and mass (Wajsowicz and Schopf, 2001). This implies that the AIPOcean data may be potentially useful to study the air–sea interaction in the Indian Ocean. AIPOcean is also useful for ENSO-related studies (Wang and Zhou, 2012). More studies are required to further explore the air–sea interaction phenomenon via AIPOcean.

Acknowledgements. This work was supported by the 973 Program (Grant No. 2010CB950401), the Chinese Academy of Sciences' Project "Western Pacific Ocean System: Structure, Dynamics and Consequences" (Grant No. XDA11010405) and the National Natural Science Foundation of China (Grant No. 41176015).

REFERENCES

Banks, H. T., 2000: Indonesian Throughflow in a coupled climate model and the sensitivity of the heat budget and deep overturning. *J. Geophys. Res.*, **105**(C11), 26 135–26 150.

Bentsen, M., G. Evensen, H. Drange, and A. D. Jenkins, 1999: Coordinate transform on a sphere using conformal mapping. *Mon. Wea. Rev.*, **127**, 2733–2740.

Bertino, L., and K. A. Lisæter, 2008: The TOPAZ monitoring and prediction system for the Atlantic and Arctic Oceans, *J. Operat. Oceanogr.*, **2**, 15–18.

Bleck, R., C. Rooth, D. M. Hu, and L. T. Smith, 1992: Salinity-driven thermocline transients in a wind-and thermohaline-forced isopycnic coordinate model of the North Atlantic. *J. Phys. Oceanogr.*, **22**, 1486–1505.

Carton, J. A., G. Chepurin, and X. H. Cao, 2000: A simple ocean data assimilation analysis of the global upper ocean 1950–95.

Part II: Results. *J. Phys. Oceanogr.*, **30**(2), 311–326.

Cummings, J. A., 2005: Operational multivariate ocean data assimilation. *Quart. J. Roy. Meteor. Soc.*, **131**, 3583–3604.

Ducet, N., P. Y. Le Traon, and G. Reverdin, 2000: Global high-resolution mapping of ocean circulation from TOPEX/Poseidon and ERS-1 and -2. *J. Geophys. Res*., **105**, 19 477–19 498.

Emanuel, K. A., 1986: An air-sea interaction theory for tropical cyclones. Part I: Steady-state maintenance. *J. Atmos. Sci.*, **43**, 585–605.

Emanuel, K. A., 1999: Thermodynamic control of hurricane intensity. *Nature*, **401**, 665–669.

Evensen, G., 2003: The Ensemble Kalman Filter: Theoretical formulation and practical implementation. *Ocean Dynamics*, **53**, 343–367.

Fu, W. W., J. Zhu, and C. X. Yan, 2009a: A comparison between 3DVAR and EnOI techniques for satellite altimetry data assimilation. *Ocean Modelling*, **26**(3–4), 206–216.

Fu, W. W., J. Zhu, C. X. Yan, and H. L. Liu, 2009b: Toward a global ocean data assimilation system based on ensemble optimum interpolation: Altimetry data assimilation experiment. *Ocean Dynamics*, **59**, 587–602, doi: 10.1007/s10236-009-0206-5.

Fujii, Y., and M. Kamachi, 2003: Three-dimensional analysis of temperature and salinity in the equatorial Pacific using a variational method with vertical coupled temperature-salinity empirical orthogonal function modes. *J. Geophys. Res*., **108**(C9), 3297, doi: 10.1029/2002JC001745.

Gaspari, G., and S. E. Cohn, 1999: Construction of correlation functions in two and three dimensions. *Quart. J. Roy. Meteor. Soc.*, **125**, 723–757.

Godfrey, J. S., and A. J. Weaver, 1991: Is the Leeuwin Current driven by Pacific heating and winds? *Progress in Oceanography*, **27**, 225–272.

Gordon, A. L., 1986: Interocean exchange of thermocline water. *J. Geophys. Res.*, **91**, 5037–5046.

Gordon, A. L., and Coauthors, 2009: The Indonesian throughflow during 2004–2006 as observed by the INSTANT program. *Dyn. Atmos. Oceans*, **50**(2), 115–128.

Han, G. J., and Coauthors, 2011: A regional ocean reanalysis system for coastal waters of China and adjacent seas. *Adv. Atmos. Sci.*, **28**(3), 682–690, doi: 10.1007/s00376-010-9184-2.

Han, G. J., H. L. Fu, X. F. Zhang, W. Li, X. R. Wu, X. D. Wang, and L. X. Zhang, 2013: A global ocean reanalysis product in the China Ocean Reanalysis (CORA) project. *Adv. Atmos. Sci.*, **30**(6), 1621–1631, doi: 10.1007/s00376-013-2198-9.

Hirst, A. C., and J. S. Godfrey, 1993: The role of the Indonesian throughflow in a global ocean GCM. *J. Phys. Oceanogr.*, **23**, 1057–1086.

Jaimes, B., and L. K. Shay, 2009: Mixed layer cooling in mesoscale oceanic eddies during Hurricanes Katrina and Rita. *Mon. Wea. Rev*., **137**, 4188–4207, doi: 10.1175/2009MWR2849.1.

Lee, T., I. Fukumori, D. Menemenlis, Z. F. Xing, and L.-L. Fu, 2002: Effects of the Indonesian throughflow on the Pacific and Indian Oceans. *J. Phys. Oceanogr.*, **32**(5), 1404–1429.

Legates, D. R., and C. J. Willmott, 1990: Mean seasonal and spatial variability in gauge-corrected, global precipitation. *Int. J. Climatol*., **10**, 111–127.

Le Traon, P. Y., F. Nadal, and N. Ducet, 1998: An improved mapping method of multisatellite altimeter data. *Journal of Atmospheric and Oceanic Technology*, **15**, 522–534.

Li, X. C., J. Zhu, Y. G. Xiao, and R. W. Wang, 2010: A model-based observation-thinning scheme for the assimilation of high-resolution SST in the shelf and coastal seas around China. *Journal of Atmospheric and Oceanic Technology*, **27**, 1044–1058.

Lin, I.-I., C.-C. Wu, K. A. Emanuel, I.-H. Lee, C.-R. Wu, and I.-F. Pun, 2005: The interaction of supertyphoon Maemi (2003) with a warm ocean eddy. *Mon. Wea. Rev*., **133**(9), 2635–2649.

Lin, I.-I., C.-H. Chen, I.-F. Pun, W. T. Liu, and C.-C. Wu, 2009: Warm ocean anomaly, air sea fluxes, and the rapid intensification of tropical cyclone Nargis (2008). *Geophys. Res. Lett.*, **36**, L03817, doi: 10.1029/2008GL035815.

Martin, M. J., A. Hines, and M. J. Bell, 2007: Data assimilation in the FOAM operational short-range ocean forecasting system: A description of the scheme and its impact. *Quart. J. Roy. Meteor. Soc.*, **133**, 981–995.

McPhaden, M. J., and Coauthors, 1998: The tropical ocean-global atmosphere observing system: A decade of progress. *J. Geophys. Res.*, **103**(C7), 14 169–14 240.

McPhaden, M. J., and Coauthors, 2009: RAMA: The research moored array for African-Asian-Australian monsoon analysis and prediction. *Bull. Amer. Meteor. Soc.*, **90**, 459–480.

Oke, P. R., G. B. Brassington, D. A. Griffin, and A. Schiller, 2008: The Bluelink Ocean Data Assimilation System (BODAS). *Ocean Modelling*, **21**, 46–70, doi: 10.1016/j.ocemod.2007.11.002.

Pandey, V. K., V. Bhatt, A. C. Pandey, and I. M. L. Das, 2007: Impact of Indonesian throughflow blockage on the southern Indian ocean. *Current Science*, **93**, 399–406.

Reynolds, R. W., T. M. Smith, C. Y. Liu, D. B. Chelton, K. S. Casey, and M. G. Schlax, 2007: Daily high-resolution-blended analyses for sea surface temperature. *J. Climate*, **20**, 5473–5496.

Salonen, K., H. Järvinen, G. Haase, S. Niemelä, and R. Eresmaa, 2009: Doppler radar radial winds in HIRLAM. Part II: Optimizing the super-observation processing. *Tellus A*, **61**, 288–295.

Schneider, N., 1998: The Indonesian throughflow and the global climate system. *J. Climate*, **11**, 676–689.

Schneider, N., and T. P. Barnett, 1997: Indonesian throughflow in a coupled general circulation model. *J. Geophys. Res.*, **102**, 12 341–12 358.

Seko, H., T. Kawabata, T. Tsuyuki, H. Nakamura, K. Koizumi, and T. Iwabuchi, 2004: Impacts of GPS-derived water vapor and radial wind measured by Doppler radar on numerical prediction of precipitation. *J. Meteor. Soc. Japan*, **82**, 473–489.

Shay, L. K., G. J. Goni, and P. G. Black, 2000: Effects of a warm oceanic feature on Hurricane Opal. *Mon. Wea. Rev.*, **128**, 1366–1383.

Teague, W. J., M. J. Carron, and P. J. Hogan, 1990: A comparison between the generalized digital environmental model and Levitus climatologies. *J. Geophys. Res.*, **95**, 7167–7183.

Wajsowicz, R., 2002: Air-sea interaction over the Indian Ocean due to variations in the Indonesian throughflow. *Climate Dyn.*, **18**, 437–453.

Wajsowicz, R. C., and E. K. Schneider, 2001: The Indonesian throughflow's effect on global climate determined from the COLA coupled climate system. *J. Climate*, **14**, 3029–3042.

Wajsowicz, R. C., and P. S. Schopf, 2001: Oceanic influences on the seasonal cycle in evaporation rate over the Indian Ocean. *J. Climate*, **14**, 1199–1226.

Walker, N. D., R. R. Leben, and S. Balasubramanian, 2005: Hurricane-forced upwelling and chlorophyll *a* enhancement

within cold-core cyclones in the Gulf of Mexico. *Geophys. Res. Lett*., **32**, L18610, doi: 10.1029/2005GL023716.

Walker, N. D., and Coauthors, 2014: Slow translation speed causes rapid collapse of northeast Pacific Hurricane Kenneth over cold core eddy. *Geophys. Res. Lett.*, **41**(21), 7595–7601, doi: 10.1002/2014GL061584.

Wang, D. X., Y. H. Qin, X. J. Xiao, Z. Q. Zhang, and F. M. Wu, 2012: Preliminary results of a new global ocean reanalysis. *Chinese Science Bulletin*, **57**(26), 3509–3517, doi: 10.1007/s11434-012-5232-x.

Wang, L., and T.-J. Zhou, 2012: Assessing the quality of regional ocean reanalysis data from ENSO signals. *Atmos. Oceanic Sci. Lett.*, **5**, 55–61.

Wijffels, S. E., J. Willis, C. M. Domingues, P. Barker, N. J. White, A. Gronell, K. Ridgway, and J. A. Church, 2008: Changing expendable bathythermograph fall rates and their impact on estimates of Thermosteric sea level rise. *J. Climate*, **21**, 5657–5672, doi: 10.1175/2008JCLI2290.1

Willis, J. K., J. M. Lyman, G. C. Johnson, et al., 2009: *In situ* data biases and recent ocean heat content variability. *J. Atmos. Oceanic Technol*., **26(4)**, 846–852.

Wu, C.-C., C.-Y. Lee, and I.-I. Lin, 2007: The effect of the ocean eddy on tropical cyclone intensity. *J. Atmos. Sci.*, **64**, 3562–3578.

Xiao, X. J., D. X. Wang, C. X. Yan, and J. Zhu, 2008: Evaluation of a 3dVAR system for the South China Sea. *Progress in Natural Science*, **18**, 547–554.

Xie, J. P., and J. Zhu, 2010: Ensemble optimal interpolation schemes for assimilating Argo profiles into a hybrid coordinate ocean model. *Ocean Modelling*, **33**, 283–298.

Yan, C.-X., and J. Zhu, 2010: The impact of "bad" Argo profiles on an ocean data assimilation. *Atmos. Oceanic Sci. Lett.*, **3**(2), 59–63.

Zheng, Z.-W., C.-R. Ho, and N.-J. Kuo, 2008: Importance of pre-existing oceanic conditions to upper ocean response induced by Super Typhoon Hai-Tang. *Geophys. Res. Lett*., **35**, L20603, doi: 10.1029/2008GL035524.

Zheng, Z.-W., C.-R. Ho, Q. N. Zheng, Y.-T. Lo, N.-J. Kuo, and G. Gopalakrishnan, 2010: Effects of preexisting cyclonic eddies on upper ocean response to Category 5 typhoons in the western North Pacific. *J. Geophys. Res*., **115**, C09013, doi: 10.1029/2009JC005562.

Zu, T. T., D. X. Wang, C. X. Yan, I. Belkin, W. Zhuang, and J. Chen, 2013: Evolution of an anticyclonic eddy southwest of Taiwan. *Ocean Dynamics*, **63**, 519–531.